Soft Matter

PAPER

View Article Online
View Journal

Cite this: DOI: 10.1039/c5sm02353j

Lack of a unique kinetic pathway in the growth and decay of Pluronic micelles†

Alexandra Arranja,[a] Gilles Waton,[a] François Schosseler*[a] and Eduardo Mendes[b]

Received 18th September 2015,
Accepted 21st October 2015

DOI: 10.1039/c5sm02353j

www.rsc.org/softmatter

We report kinetic experiments on dilute brine solutions of P84, P94 and P104 Pluronic copolymer micelles. The growth and the decay of micelles after temperature steps are measured by non-standard time resolved multi-angle photon correlation spectroscopy. Several concurrent mechanisms are at work during the very slow equilibration of solutions, namely insertion/expulsion of unimers, aggregation/dissociation of micellar aggregates, and fusion/budding of micellar aggregates. Their relative rates determine both the kinetic pathways and the morphologies of the micellar assemblies, which depend markedly on modest changes in the copolymer molecular weight. For the typical Pluronic copolymers investigated here, none of these elementary processes can be neglected if the resulting morphology is to be explained. This feature imposes multiple kinetic behaviours where growth and decay of Pluronic micelles become strongly dependent on the thermal history. We point out to some possible shortcomings in the studies of micellar growth kinetics by light scattering techniques. Extensive time-resolved multiangle measurements are a prerequisite for avoiding these pitfalls.

1 Introduction

The dynamics of block copolymer micelles in a selective solvent of one block (A) has been the subject of intensive work in the past two decades.[1–3] The polymerization index P_B and the more or less poor quality of the solvent, as quantified by the Flory χ_B interaction parameter,[4] for the insoluble block (B) are key parameters that govern the dynamics. Thermodynamic equilibrium can be achieved only for not too large values of the product $\chi_B P_B$ that determines the precipitation of the insoluble block. Also large values of P_B increase dramatically the characteristic time for the equilibration of the micellar core. The incompatibility between the two components, as measured by $\chi_{AB} P_A P_B$, plays also a major role in the dynamics.[5] Here χ_{AB} is the interaction parameter between the two components. Thus, by varying all these parameters, a continuum of behaviours can be obtained between the polymer micelles at full thermodynamic equilibrium and the frozen micelles that can be assembled only through progressive solvent exchange.[6]

At thermodynamic equilibrium, there is a fast exchange of unimers between the micelles and the bulk solution through insertion/expulsion steps like in short surfactant solutions.[7] In comparison, fusion/fission of micelles is relatively much slower and plays usually a minor role in equilibrium dynamics.[8–18]

After small temperature jumps, the concentration of free surfactant molecules (cmc) increases to a new value and the size and number density of copolymer micelles achieve new average values. The cmc is equilibrated rapidly through the fast exchange of unimers between the bulk solution and the micelles.

The equilibration of the average number density of micelles is slower by two or three orders of magnitude and its mechanism was the subject of much discussion.[19–30] Two different routes based on the equilibrium dynamics have been proposed: step by step association of individual unimers or successive fusion/fission steps between micellar aggregates.

For appropriate block length ratios, spherical micelles can grow reversibly into wormlike micelles upon changes in temperature[31–39] or solvent composition.[40,41] The equilibration times vary widely in the range of 1–100 h with experimental conditions and various kinetic pathways were proposed for growth transition: fusion/fission coexisting with unimer exchange,[34] random fusion/fragmentation of spherical and rodlike micelles,[37] or aggregation of spherical micelles followed by transformation into smooth cylinders.[40] The worm-to-sphere decay transition is consistently faster than the growth[33,39,40] and facilitated by higher polymer concentration.[39] Mechanisms proposed for decay transition were either a sequential budding at rod ends followed by spherical micelles release[39,40] or fast random fragmentation followed by equilibration through unimer exchange.[41]

While each of these mechanisms has been proposed and validated for specific systems, only a few systematic variations of molecular parameters like, *e.g.*, molecular weight or composition

[a] Institut Charles Sadron, University of Strasbourg, CNRS UPR 22, 23 rue du Loess, 67034 Strasbourg Cedex 2, France. E-mail: francois.schosseler@ics-cnrs.unistra.fr; Fax: +33 (0)3 88 41 40 99; Tel: +33 (0)3 88 41 40 39

[b] Delft University of Technology, Department of Chemical Engineering, Advanced Soft Matter, Julianalaan 136, 2628 BL, Delft, The Netherlands

† Electronic supplementary information (ESI) available: Purification and characterization of copolymers (SEC, NMR, and DSC). Details and discussion about data analysis. Discussion of crossover effects. Some specific results. See DOI: 10.1039/c5sm02353j

have been performed to determine how the latter affect the relative importance of these mechanisms. Moreover, some light scattering studies did not separate properly the growth kinetics from the crossover to the entangled regime and/or out of the Guinier regime for the growing micelles. Therefore conclusions, *e.g.*, about concentration effects on the kinetics, could be strongly biased by these approximations.

Here we address these issues by studying the growth kinetics of dilute Pluronic micelles by multi-angle light scattering experiments. Pluronics are commercial EO_x–PO_y–EO_x copolymers (where EO = ethylene oxide and PO = propylene oxide) that form micelles with a PO core in aqueous solutions.[42–44] We study specifically the effect of the total molecular weight of the copolymers while keeping their EO/PO composition constant and we perform small temperature jumps in the transition region where the spherical micelles start to grow into elongated cylinders.

2 Experimental

Polymer purification and characterization

Pluronics P84, P94 and P104 were kindly provided by BASF. Size exclusion chromatography (SEC) analysis of these samples revealed the presence of satellite peaks in the distributions of molecular weights for the three samples. Since such impurities have been reported to critically modify the micellization behaviour,[26,45,46] we purified the samples by dialysis and succeeded to remove all or most of these satellite peaks. Details about purification and characterization of the samples by SEC, NMR and DSC are given in the ESI.† Table 1 gives the main characteristics of the purified samples.

Sample preparation

Solutions were prepared at polymer concentration $C_p = 0.5$ g L^{-1} by weighing the purified polymer in 2 M NaCl brine prepared with MilliQ water. Gentle manual shaking was applied to facilitate dispersion and samples were immediately placed in the fridge (*ca.* 4 °C) before use. We use a brine solvent since added salt is known to shift transition temperatures down closer to room temperature in PEO based systems.[47]

Photon correlation spectroscopy (PCS)

All samples were filtered (Millipore hydrophilic PTFE 0.45 μm) in the cylindrical scattering cells (diameter 20 mm) prior to the PCS experiments, which were performed using a compact ALV/CGS-8 goniometer system equipped with an He–Ne laser (14 mW, λ = 632.8 nm, vertically polarized), an ALV-7002/USB-25 autocorrelator and an automatic attenuator driven using the proprietary ALV software.

Table 1 Characteristics of the samples

Sample	M_n[a]	M_n[b]	% PEO[b]	n_{PPO}[c]	cmT[d]	T_1[d]	T_2[d]
P84	4800	4700	43	46	10	31	—
P94	5200	5000	45	48	9	28	32
P104	8100	6300	39	66	2	30	34

[a] SEC. [b] NMR. [c] Polymerization index of PPO block ESI. [d] °C at 0.5 g L^{-1} with 2 M NaCl, defined in the text.

The temperature of the matching index fluid (toluene) was controlled using a circulating water bath (Huber) and measured using a Pt probe. Temperature was stable within ±0.1 °C and temperature jumps were achieved after about two minutes.

Measurements were done by looping repeatedly on nine scattering angles ($20° \leq \theta \leq 120°$) and measuring the intensity correlation function (ICF) and the average scattering intensity I_{meas} for typically 180 s at each angle.

The effective incident intensity I_0 was measured by a diode placed after the attenuator. For very strong scattering intensities, the incident intensity was attenuated further by neutral filters with known transmission values T_r. The total scattering intensities were calculated as $I_{tot} = I_{meas}/I_0/T_r$ and further normalized with respect to the average intensity I_{tol}/I_0 scattered by a toluene standard. All intensities in the paper are given and plotted in these units.

Kinetics was investigated for typically 1 day up to 20 days at a given temperature. Unless otherwise specified in the manuscript, samples were kept in place for the whole duration of the experiment. Therefore most gaps in the data are only due to random unattended crash of the acquisition software during measurements, with no consequence on the thermal regulation of the sample. The total duration for a complete thermal history lasted typically a few weeks. Therefore for each thermal history several thousands of ICFs were accumulated.

Data analysis

Each ICF was analyzed using CONTIN software. In most cases, we obtained one or two decay modes that could be very well described by log-normal curves. Thus the peaks in the distributions of relaxation times could be easily fitted and deconvoluted. Peak areas were then calculated and gave the relative contribution of each decay mode to the decay of the ICF and to I_{tot}.[48–50] We used the position of each peak maximum as the value of the corresponding relaxation time τ. The latter was converted into an apparent hydrodynamic radius (AHR) R with the Stokes–Einstein relation to factor out any trivial temperature dependence due to the Boltzmann factor k_BT and to the solvent viscosity $\eta(T)$:

$$R = \frac{q^2 k_B T}{6\pi\eta(T)}\tau \quad (1)$$

where $q = (4\pi n/\lambda)\sin(\theta/2)$ is the scattering vector. Eqn (1) should ensure q-independent AHRs for diffusive decay modes. However, this is not always true in some special conditions like, *e.g.*, out of the Guinier regime when $qR > 1$ and internal dynamic modes come into play for long wormlike micelles,[51] or when the size polydispersity is large (ESI†).

The results of the deconvolution were checked by bi-exponential fits when the overlap of decay modes was important. See ESI,† for further details about data analysis and for a discussion about biases introduced by cumulants or bi-exponential fits.

3 Results

Samples stored in the fridge were first brought to 25 °C. As this temperature is above the critical micellar temperature (cmT) for

the three copolymers at this concentration in this solvent (2 M NaCl) (ESI†), spherical micelles are expected. Interestingly the total scattering intensity I_{tot} can exhibit very slow non-monotonic transients depending markedly on the scattering angle. It can take several hours up to days to stabilize. The kinetics of micellization depends on both the molecular weight and the thermal history of the samples. Its detailed study is postponed to a future paper.

The hydrodynamic radii of the spherical micelles, R_{sm}, measured before the subsequent temperature steps rank as expected with the molecular weight of the unimers: $R_{sm} \approx 7.1 \pm 0.1$ nm for P84, $R_{sm} \approx 8.0 \pm 0.5$ nm for P94 and $R_{sm} \approx 9.3 \pm 0.2$ nm for P104. Their weight averaged aggregation numbers N_{sm} obtained from the light scattering intensities are about 70, 80, and 110 for P84, P94, and P104, respectively.

Total scattering intensity

For the three copolymers, an increase of I_{tot} by about two orders of magnitude is obtained for temperature increases of about a few degrees (Fig. 1). First moderate, the increase becomes much more pronounced above a temperature T_1 where the onset of angular dependence also indicates the progressive appearance of large objects in the solution. Thus T_1 corresponds roughly to the onset of micellar growth. Then, above a temperature $T_2 > T_1$, I_{tot} becomes insensitive to temperature and the angular dependence stops increasing with temperature. This can be due to a cross-over to either the entangled regime of wormlike micelles or the intermediate scattering regime of large aggregates ($qR > 1$). In both cases, the scattering intensity should become independent of the aggregate sizes.[52] For P84 this regime was not obtained in the temperature range investigated, but for P94 and P104, T_2 is about 32 °C and 34 °C, respectively. Therefore, in the following, we have restricted our analysis of growth to a limited range of temperatures above T_1, as shown by gray rectangles in Fig. 1. Although T_1 depends weakly on the copolymer molecular weight (Table 1), there are striking differences between the behaviours of the three copolymers.

The most evident is the stepped increase of I_{tot} for P84 as compared to the continuous increase observed for P94 and P104. After each temperature jump applied above 30 °C to the P84 solution, there is first a step increase of I_{tot} followed by a slower and smaller increase, which does not reach a real steady state even after 24 hours (≈1500 min). Conversely, under the same conditions, P94 and P104 solutions do not depart from a smooth increase of I_{tot} and display merely a faster rate of intensity increase at higher temperatures. The time evolution of the angular dependence follows the same pattern as that of I_{tot}: it varies abruptly for P84 (Fig. S11, ESI†) but very progressively for P94 (Fig. S11 and S12, ESI†) and P104 (Fig. S13, ESI†) after a temperature change.

Analysis of the intensity correlation functions (ICF)

CONTIN analysis of the ICFs measured in the range $T_1 \leq T \leq T_2$ shows that the onset of growth is associated with the presence of two decay modes for all three copolymers. However, the behaviour of these two decay modes as a function of temperature and time depends strikingly on the molecular weight. These decay modes, labeled for convenience as fast and slow, correspond to two different populations of micellar aggregates.

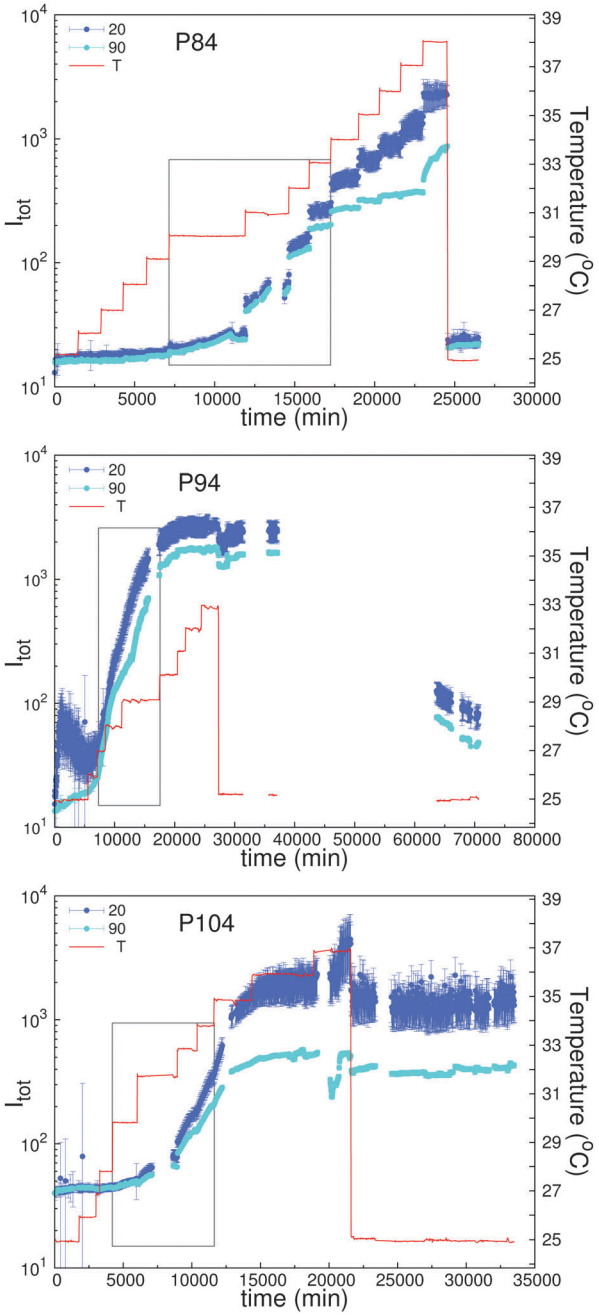

Fig. 1 Evolution of total scattering intensity with time and temperature for copolymers P84 (top), P94 (middle), and P104 (bottom) for two scattering angles, θ = 20° and 90°. Other angles are omitted for the sake of clarity. The red lines are the temperature steps. Grey rectangles show the regions used for the growth analysis. Error bars are the standard deviation in I_{tot} during ICF measurements.

For P84 (Fig. 2), after a moderate continuous increase of both the scattering intensity and the hydrodynamic radius between 25 °C and 30 °C, there is a sudden jump in these quantities at 31 °C (≈12 000 min). When the temperature is increased further to 32 °C (≈14 500 min), a second slower decay

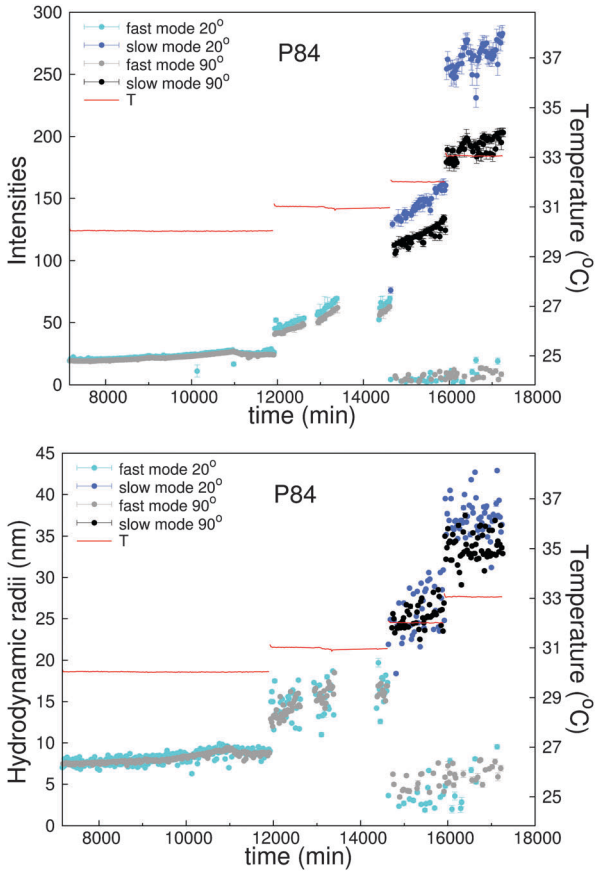

Fig. 2 Evolution with time and temperature of the intensities (top) and apparent hydrodynamic radii (bottom) associated with the fast and the slow decay modes for sample P84, $\theta = 20°$ and 90°. Error bars as explained in the ESI.†

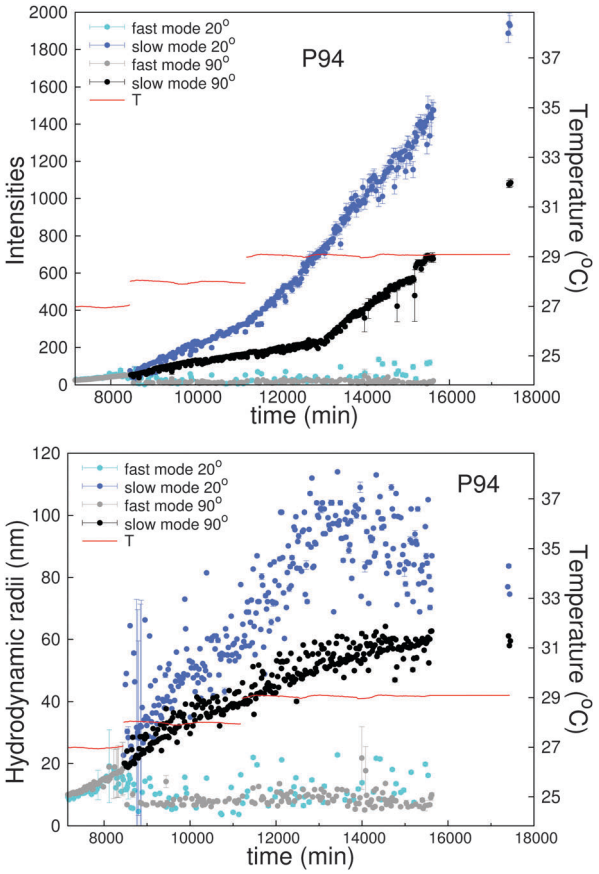

Fig. 3 The same as Fig. 2 for sample P94.

mode with a much larger and q-dependent scattering intensity appears almost instantaneously. At 33 °C (≈16 000 min), the scattering intensity of the slow mode and its q-dependence are increasing further while the associated AHR also becomes q-dependent. The faint fast decay mode persisting above 31 °C (≈14 700 min) corresponds to smaller scattering intensities (≈2 a.u.) and hydrodynamic radii (≈5 nm) than those measured for the spherical micelles before the onset of growth, resp. ≈16 a.u. and ≈7 nm before ≈12 000 min. At $T = 31$ °C, it is likely that the respective contributions of spherical micelles and growing micelles could not be separated by CONTIN. Indeed, for this temperature, bi-exponential fits yielded satisfactory results as well with $R_{fast} \approx 8$ nm and $R_{slow} \approx 20$ nm.

For P94 (Fig. 3), no jump is observed in the scattering intensity, which increases smoothly at a rate that grows with temperature. At 28 °C (≈8500 min), a second slower mode appears: its associated scattering intensity and hydrodynamic radius as well as its q-dependence increase progressively with time. This behaviour becomes more pronounced at 29 °C (≈11 000 min) (see also Fig. S12, ESI†). When R_{slow} increases above 30–40 nm its values become progressively q-dependent and T-independent (Fig. 3, bottom). This occurs first for the largest angle and then progressively at smaller angles. At an elapsed time of around 13 000 min, the rate of intensity increase becomes suddenly larger for the largest scattering angles and the q-dependence that was steadily increasing strikingly shrinks back to its value at the beginning of the temperature step (Fig. S12, ESI†). Thus the micelles start their growth and enter the entangled regime in a very narrow temperature interval of about 1–2 °C. As the relative contribution of the slow decay mode increases, the reliable characterization of the fast decay mode becomes more difficult. Although rather dispersed, values for $I_{fast} \approx 15$ a.u. and $R_{fast} \approx 5$–10 nm still remain mostly consistent with those measured at 25 °C.

Although P104 exhibits the same continuous intensity increase as P94, the behaviour of the decay modes is very different (Fig. 4). The slow decay mode appears progressively at 32 °C (≈6000 min). Since it corresponds immediately to large apparent hydrodynamic radii ($R_{slow} \approx 100$ nm), it can only be detected first at small scattering angles. At 33 °C (≈9000 min) and 34 °C (≈10 500 min), it is clearly seen at all scattering angles and the associated R_{slow} values show a marked q-dependence (see also Fig. S13, ESI†) For these two temperatures, the results shown are obtained with bi-exponential fits of the ICFs, which reduce the dispersion of the data points. In contrast to P84 and P94, both I_{fast} and R_{fast} still increase slightly in this regime (Fig. S13, ESI†). They decrease only at higher T (not shown) to values $I_{fast} \approx 15$ a.u and $R_{fast} \approx 7$–8 nm slightly smaller than those measured at 25 °C (resp., ≈40 a.u. and ≈9 nm).

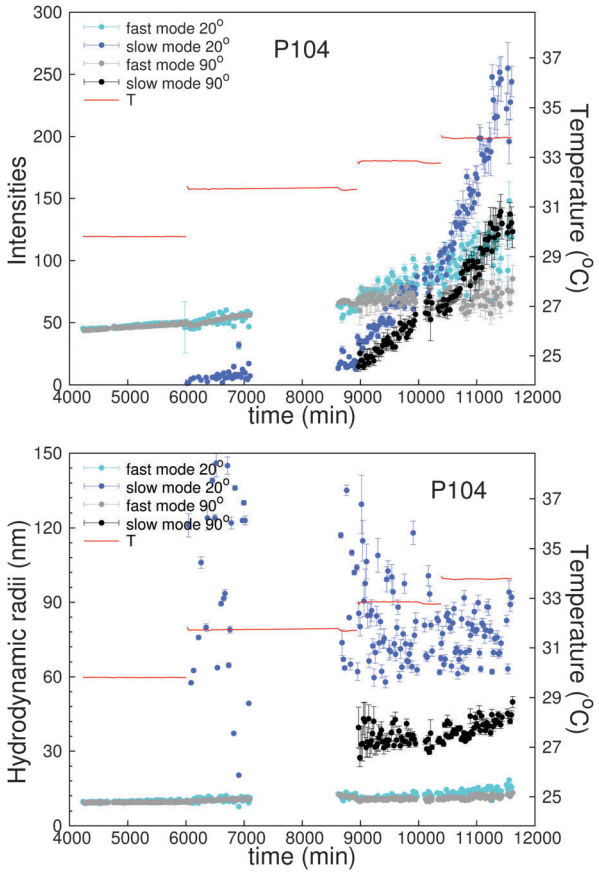

Fig. 4 The same as Fig. 2 for sample P104. Plotted results from CONTIN analysis except those at 33 and 34 °C from bi-exponential fits.

Neglecting the fraction of unimers in the spherical micelles, we get rough lower estimations for the mean aggregation numbers of the large objects about 1100, 8900, and 650 for P84 (33 °C), P94 (29 °C), and P104 (34 °C), respectively.

Stability after temperature decrease

We also tested the evolution of the solutions when they were cooled down to 25 °C. Again the three copolymer solutions showed strikingly different evolutions.

In the P84 solution (Fig. 1, top), I_{tot} values measured at all angles decreased back to values close to the ones measured at the beginning of the experiment in the time needed to cool down the sample (a few minutes) with only one decay mode and $R_{fast} \approx 8$ nm, slightly larger than before the T-steps ($\approx$7 nm).

In the P94 solution (Fig. 1, middle), the intensity and radius values associated with each decay mode remained nearly constant for one week, with only a small 10% decrease in I_{slow}. After this time, the sample was kept at 25 °C in a different bath for 18 days and then measured again for 5 days. Even after one month at T = 25 °C this sample did not fully return back to its initial state at this temperature: I_{tot} values were still about one order of magnitude larger than the initial ones, two decay modes were present, the faster one with characteristics corresponding to the initial state and the slowest one, which is responsible for the excess of intensity, corresponding to $R_{slow} \approx 150$ nm, larger than the value measured at T = 33 °C.

The total scattering intensity and the two decay modes in the P104 solution displayed the same stability as in the P94 solution during 8.5 days after cooling down (Fig. 1, bottom).

4 Discussion

General remarks about crossover artefacts

As micellar aggregates start to grow, I_{tot} becomes progressively q-dependent, as expected, and this angular dependence is entirely due to I_{slow} contribution. For large enough aggregates, R_{slow} values also show a q-dependence (Fig. 2–4), which can be due to flexibility and/or size polydispersity.

For flexible objects, both the conformational fluctuations as well as the translational diffusive motion contribute to the fluctuations of concentration. The former contribution dominates for large objects with low translational diffusion coefficient and the decay rate of the ICF crossover to a q^3 scaling,[51,53] which yields a q-dependent apparent hydrodynamic radius (AHR) $R_{slow} \approx q^{-1}$ unrelated to the true size of the Brownian objects (see ESI,† III.1 for details).

Large size polydispersity can also yield q-dependent AHRs since the relative contributions of the Brownian objects to the ICF are weighted by their scattering intensity: the largest objects contribute more at smaller q values while the smallest objects are the major contributors at larger q values. Therefore the sampling of the objects shifts with their growth and only average values extrapolated at q = 0 keep a precise definition while those measured at fixed angles are poorly defined (see ESI,† III.2 for an illustration).

Whatever the reason, q-dependent AHRs are the warning sign that the measured values are only loosely related to the true average size of the aggregates. Therefore, following the kinetics of growth with intensity or radius values measured at a fixed and large scattering angle can be misleading. These aspects were overlooked in former studies.[34–38]

Above a certain temperature and/or after a certain time, all samples become insensitive to further T-steps with constant I_{tot}, I_{slow}, and R_{slow} values within experimental errors. This behaviour can mark the transition to an entangled regime where the elongated micelles overlap and I_{tot} becomes independent of their length.[52] The single characteristic length is then the mesh size of the entangled solution, $\xi \sim C_p^{-3/4}$, which decreases with concentration. T-jump experiments bringing the solutions into this regime will display faster relaxations to $R_{slow} \approx \xi$ independent of the true micellar size. These effects were also neglected in some earlier studies[36,37] at higher concentrations. Significantly, in one case,[36] the viscosity, which is sensitive to the true size of the entangled micelles, still increased after I_{tot} reached a stationary value.

For these reasons, we have based our discussion in the T-range where the samples displayed a clear sensitivity to temperature steps, and on values measured at the smallest scattering angles,

which can be considered as good approximations to values extrapolated at $q = 0$.

Kinetic pathways of micellar growth

Fig. 2–4 show a first clear difference between P84 solutions on one hand and P94 or P104 solutions on the other hand. After each temperature step, the P84 solutions display a sudden increase of intensities and radii followed by a moderate increase on much longer timescales. Therefore mean micellar sizes corresponding to some close-to-equilibrium states can be defined as a function of temperature. On the other hand, for P94 and P104 solutions, the growth appears continuous with rates increasing with temperature. It seems that no equilibrium state is achieved for P94 and P104 within 1 or 2 days, at least for this polymer concentration. All samples are very sensitive to temperature in the range $T_1 < T < T_2$ and small 1 °C steps induce a noticeable change in the behaviour.

It can be emphasized that the hydrodynamic radius of P84 and P94 unimers is about the same (resp. 1.9 ± 0.2 nm and 1.6 ± 0.2 nm). Therefore the diffusion of unimers cannot explain the different orders of magnitude for the equilibration times. The structure function of either P94 or P104 solutions depends on their thermal history, hence on the experimental protocol. This feature allows only a qualitative comparison of their growth kinetics and morphologies but the design of an experimental protocol that would allow a more quantitative comparison between the three different copolymers would be very difficult to justify. For these reasons, we just chose a reasonable duration of the order of 24 hours for P94 and P104 solutions. For P84 solutions, the duration of each temperature step does not really matter as long as it is close to the equilibrium state.

Despite the strong difference in kinetics, all solutions share the same feature: small spherical micelles can still be detected while larger species appear in the solution. The spherical micelles are about the same size as before the micellar growth (R_{sm} values above) in P104 solutions and slightly smaller in P84 and P94 solutions. Within experimental accuracy, the associated I_{fast} values remain in the same order of magnitude as the contribution of spherical micelles before the growth transition. Therefore the number density of small micelles remains in the same order of magnitude as below the growth transition. This remains true at higher temperatures even above T_2 (not shown). This suggests that the phase diagram region explored in this study corresponds to the coexistence of spherical micelles and larger aggregates.

The population of growing aggregates is clearly different for the three copolymers. Increasing T the solutions of P84 and P94 show a progressive splitting of the two decay mode intensities, both being comparable at the onset of growth. There is also a progressive increase of R_{slow} and of the q dependence of the slow mode characteristics. These features indicate a progressive increase of the micellar size, through either unimer exchange or fusion of spherical micelles.

In contrast, the onset of intensity growth in P104 is due to the appearance of a slow mode characterized by a large $R_{slow} \approx$ 100 nm associated with a small but strongly q-dependent intensity contribution $I_{slow}/I_{fast} \approx 0.1$. As I_{slow} increases R_{slow} remains about the same. At the same time, there is a modest increase of I_{fast} and R_{fast}. At later times ($\approx$10 000 min) I_{fast} starts to display a small q-dependence. This suggests two concurrent processes triggered by the temperature increase, the progressive formation of large spheroidal aggregates composed by many spherical micelles and the growth of slightly elongated micelles. There are only a few large spheroidal aggregates and the growth of spherical micelles ($R_{fast} \approx 9$ nm) yields only weakly elongated micelles ($R_{fast} \approx 12$ nm).

The different morphologies of the large aggregates are further confirmed by the ratio of their radius of gyration to their hydrodynamic radius. It is about 1.6 ± 0.2, 1.7 ± 0.3, and 1.2 ± 0.2 for, respectively, P84 (33 °C), P94 (29 °C), and P104 (34 °C). The smaller value for P104 is consistent with a more compact structure of the large aggregates in this sample.

The above findings can be rationalized by the effect of unimer molecular weight on the prevailing kinetic pathway of the sphere-to-rod transition. Previous studies on spherical copolymer micelles have shown that the faster and dominant dynamical process at thermodynamic equilibrium is the unimer exchange[8–18] and this is also true for elongated micelles.[15] On the other hand, fusion/fission events, although much slower, must be present to explain some results.[18] As the molecular weight of the unimers increases, their exchange will be slowed down by the smaller concentration of free unimers[54] and/or the higher energy barrier experienced by them to cross the shell.[15,30] Here the latter one should be proportional to the polymerization degree n_{PPO} of the insoluble block.[15] Then the much slower fusion/fission of micellar aggregates can become a significant competitor.[27] However, with a further increase of the molecular weight of the insoluble block, the aggregation number of the spherical micelles N_{sm} increases and the equilibration of aggregated spherical micelles into smooth cylinders[40] should become progressively very difficult because it involves many intramicellar rearrangements.

These features can well explain the shift in the behaviours displayed by the three copolymers with increasing molecular weight. After T-jumps the smaller P84 displays a fast adjustment of the average size of the micellar aggregates followed by a much slower equilibration. This is consistent with previous measurements with a classical T-jump setup.[24,28] For P84 solutions with low salt concentration, the characteristic time for unimer exchange was shown to be a few 10 μs and a second longer relaxation time ($\approx$1 s) was attributed to fusion/fission. Under high salt conditions, an additional slow size variation could be attributed to small intramicellar rearrangements.[24,28] Thus for sample P84 with $n_{PPO} \approx 46$ and $N_{sm} \approx 70$, all these processes occur concurrently and allow the two step relaxation observed in our experiments. For the slightly larger P94, the insertion/expulsion of the unimers becomes more difficult and fusion/fission events occur with much fewer intervening insertion/expulsion events. Although unimer exchange is still the faster process, the timescale of the kinetics becomes the one of the fusion/fission events because they involve a much larger transfer of matter between aggregates. The equilibration time is longer for P94 because both $n_{PPO} \approx 48$ and $N_{sm} \approx 80$ are larger

for this copolymer. For P104 micelles, still larger values $n_{PPO} \approx 66$ and $N_{sm} \approx 110$ make the intramicellar rearrangements so difficult that the fusion of two micelles becomes very unlikely. Therefore, in order to decrease the PEO/water interface, the micelles form large spheroidal aggregates without fusion. In parallel, only a modest and very slow increase in the size of the small spherical micelles can be obtained after a long time through slowed down unimer exchange.

Thus several concurrent mechanisms are at work during the equilibration of the solutions and their relative rates determine both the kinetic pathways and the morphologies of the micellar assemblies. Fig. 5 summarizes the evolution of the kinetic pathways as a function of increasing unimer molecular weight. The corresponding kinetic equations should therefore consider both unimer exchange and fusion/fission, as proposed in ref. 37, but should further distinguish the two steps in a fusion event: collision/aggregation and fusion itself, as well as in a fission event: budding of micellar aggregates and separation of aggregated buds. This complexifies considerably the model and its resolution, since as argued here, there are only a few experimental cases where some mechanisms can be neglected, like, *e.g.*, for polymer micelles at thermodynamic equilibrium where unimer exchange is the dominant process.[8–17] The full set of coupled equations should be solved with longer time series for a meaningful analysis of the present systems. This is out of the scope of this paper.

As emphasized by one referee, apart from the most obvious effect of molecular weight on the dynamics studied here, composition polydispersity has also been shown to play an important role in the equilibrium dynamics of diblock copolymer micelles.[10,13–15] It was not possible here to quantify the compositional heterogeneity of these copolymers but it is apparently not important enough to alter the expected variation with increasing molecular weight. Such effects could be investigated with tailor-made samples. However they complicate further the quantitative analysis.[15]

Stability of solutions after the temperature decrease

Surprising stability of wormlike morphologies after a decrease of the temperature back in the spherical micelle regime has already been reported for Pluronic P123 in the presence of salt.[35,36] Here the elongated micelles of P84 return back to their spherical morphology in a time shorter than the experimental resolution, which confirms that the fast unimer exchange plays also a role in the equilibration kinetics of P84 after the temperature decrease. On the other hand, the elongated micelles of P94 take much longer time periods to decay to their spherical shapes. After dilution of P94 samples following the procedures described in ref. 35 and 36, this stability is still present but for shorter time periods. Only when the samples were diluted to a polymer concentration lower than the cmc at the given temperature and salt concentration did the long micelles disappear very rapidly (results not shown). These features are consistent with the much slower fusion/fission process being the prevailing mechanism for P94. Finally the large spheroidal aggregates of spherical micelles formed in P104 solutions appear to be very stable after the temperature decrease and do not redisperse easily at low T once formed at high T. This might be due to the difficulty of water to repermeate the spheroids and to rehydrate the collapsed PEO shells.

It is worth noting that the kinetic pathways involved in the T jump from high to low temperature for P104 and P94 are likely to depend on the structure of the micellar aggregates achieved during their thermal history. For P104 aggregates, the peculiar structure deduced from the analysis of their growth introduces a new parameter, *i.e.*, the permeation of water inside the spheroidal aggregates. The permeability of these spheroids depends on their compactness and thus on the PEO dehydration state achieved at a given high temperature. One might expect that these spheroidal aggregates would be less stable if formed at a lower temperature and/or for shorter duration. For the wormlike aggregates formed by P94, this is not as likely since rehydration of the PEO corona can be achieved more easily. In this case, our results are consistent with a slow expulsion of the unimers from the core and rare fission events hindered by the lower mobility of the unimers in the core but more experiments would be needed to clarify the effect of the thermal history on their decay. Finally P84 wormlike aggregates can decay very rapidly because a new equilibrium can be achieved rapidly through the fast escape of individual unimers from the core. In this case the involved cooperativity is smaller than the one necessary to create two micellar caps in a fission event and the faster process dominates the followed kinetic pathway.

Comparison with previous studies

Such a comparison is not straightforward since many experimental aspects are different.

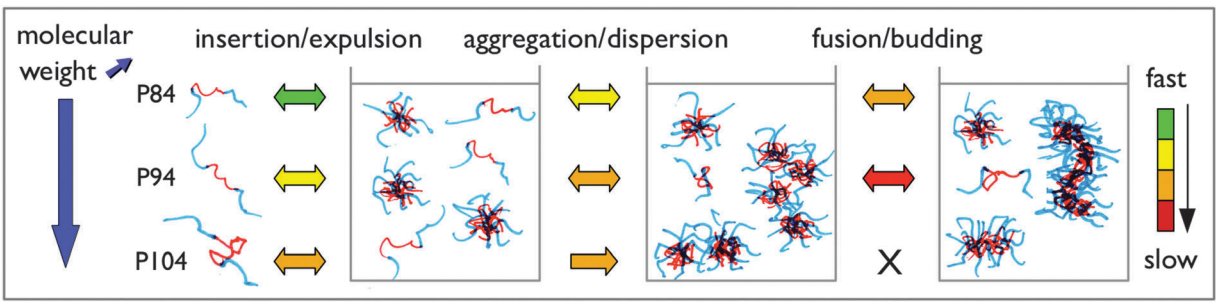

Fig. 5 Sketch of the concurrent mechanisms and the resulting kinetic pathways for increasing unimer molecular weight.

Growth kinetics of Pluronic micelles have been reported for copolymers P103,[36–38] P104,[38] P123[34,35,38] or F127[38] that have equal or larger PPO nominal block length than the samples investigated here. Therefore only our P104 sample has been studied before. However, in all previous studies, samples were used as received despite the fact that impurities have been known for a long time to have an effect on the aggregation of these copolymers. Since our P104 sample had the largest amount of smaller molecular weight impurities that was almost completely eliminated in our purification process (see ESI†), a direct comparison is not possible even in this case.

Almost all previous studies were performed in the presence of added salt[34–36] and/or added alcohol,[34,38] with the exception of ref. 37 that was done in pure water solutions. Qualitatively, all previous results converge to the conclusion that the growth proceeds faster for higher alcohol content[34,38] and lower salt content,[36] with the nature of salt being an important parameter.[36]

Our measurement techniques differ also from those used in previous studies. Here we used a combination of static and dynamic multiangle light scattering measurements. While the dynamic light scattering technique, mostly at a single scattering angle, was also used previously,[34–38] only small angle neutron scattering intensities have been performed in ref. 35, 36 and 38 *i.e.*, in a scattering vector range where the growth of large objects cannot be measured. Only ref. 37 has reported light scattering intensities but mostly at a single scattering angle.

Analysis of dynamic light scattering data was previously done by cumulants[34,37] or the modified cumulants method[35,36] although partial checks by CONTIN methods revealed in some cases[34,37,38] two decay modes in the intensity correlation functions. In ref. 38, a forced bi-exponential fit was used. This contrasts with our approach where the number of decay modes was systematically checked for all angles and all times, thanks to extensive software writing. As shown in the ESI† (Fig. S8), *a priori* assumptions on the number of decay modes can easily yield biased results.

For the above technical reasons, no experimental evidence for systematic coexistence between small spherical micelles and larger aggregates was provided by any of these previous studies. Here we show that during the growth transition of samples P84, P94, and P104, spherical micelles always coexist with larger aggregates although they can be very difficult to detect, especially at small scattering angles, due to the large intensity scattered by the larger aggregates. Moreover there is a clear size gap in the size distributions except in the very vicinity of the transition temperature.

Only one previous study[37] attempted a detailed mechanistic description of the growth using analytical kinetic models. The growth of P103 in pure water was reported by static and dynamic light scattering measurements at a single scattering angle. Consistently with their cumulants analysis used *a priori*, the authors concluded that the growth mechanism was random fusion–fragmentation, yielding an exponential size distribution with no gaps, clearly inconsistent with our data. A second striking difference is the very large scattering intensity increase measured during the growth in our systems compared to a mere factor 5 measured for P103.[37] Although part of the difference can be assigned to intensity measurements performed at 90° scattering angle in the latter case, this suggests that P103 aggregates might be more similar to the ones formed by P104 than to the true elongated micelles formed by P84 and P94.

The previous studies have reported much faster relaxations to equilibrium after *T*-jumps in the growth regime.[34–38] Several features could explain our findings:

(i) As detailed above, our copolymer samples have a different composition and have been purified from low molecular weight impurities.

(ii) Our experiments are performed at high NaCl concentration with no added alcohol, conditions that slow down the kinetics. Also our samples were not stirred like in some previous studies.[34,37]

(iii) Sometimes higher polymer concentrations[34,35,37] have likely made the leveling of intensity and AHR faster due to the transition to the entangled regime as discussed above. This feature calls for increased caution when characterizing the kinetic constants as a function of copolymer concentration, as attempted in ref. 37.

(iv) Also the AHR of large aggregates, either flexible or with a large size polydispersity, cannot be measured accurately out of the Guinier regime and the erroneous values show a misleading apparent saturation. Some previous results might have been affected by this effect,[36,37] which start to show up for AHRs about 30 nm at $\theta = 90^\circ$ using our experimental setup.

To conclude this comparison, there is convincing evidence that copolymer micelles made from P84, P94, P104, P103, P123, and even F127, can form at high temperature larger aggregates under appropriate conditions of added salt and/or alcohol. However the lack of homogeneity in the experimental conditions and in the analysis methods prevents any definitive comparisons between the exact morphologies of these aggregates. Based on our results, we suspect however that some diversity in the kinetic pathways and in the resulting morphologies has hidden behind the generic features reported so far, *e.g.*, increased viscosity, light scattering intensity or apparent hydrodynamic radius. This diversity can only be unraveled by detailed measurements using the methods reported here.

5 Conclusions

We studied the effect of copolymer molecular weight on the kinetics of growth and decay of Pluronic micelles after *T*-jumps using time-resolved multiangle photon correlation spectroscopy.

Our results demonstrate that increasing by a factor less than two the length of the insoluble PPO block at fixed PEO/PPO composition has dramatic effects on both the kinetics of equilibration and the morphologies of resulting aggregates after a *T*-jump in the growth regime: while P84 can form equilibrium wormlike micelles, the wormlike micelles formed by P94 are likely never at full equilibrium on the timescale of our experiments. With P104 only large spheroidal aggregates of spherical micelles and, on longer timescales, slightly elongated

micelles are obtained. Upon cooling the solutions down to the spherical micelles regime, wormlike micelles made from P84 return very rapidly to spherical micelles while P94 solutions remain for very long times in their high temperature state. The large spheroidal aggregates formed in P104 solutions do not redisperse easily at low temperature. For all copolymers, spherical micelles are still present at all temperatures and their concentration remains the same order of magnitude below and above the growth transition.

These results are explained by several elementary processes working concurrently to equilibrate the population of micellar assemblies after a *T*-jump, namely insertion/expulsion of unimers, aggregation/dissociation of micellar aggregates, and fusion/budding of micellar aggregates. The rates of these elementary processes depend markedly on the copolymer molecular weight at a fixed polymer concentration. In the cases investigated here, none of these processes can be safely neglected when attempting to solve the corresponding set of coupled kinetic equations, if the resulting morphology is to be taken into account. We suspect that this might also hold true for previous studies where the morphology of the micellar aggregates was not investigated thoroughly enough to distinguish a possible departure from the assumed wormlike morphology. Extensive time-resolved multiangle measurements are a prerequisite for this purpose.

Our results also point to some possible shortcomings in studies of micellar growth kinetics where the crossover to the entangled semidilute regime and/or out of the Guinier regime might yield an apparent saturation of the total scattering intensity or the hydrodynamic radius. Moreover analysis of intensity correlation functions with *a priori* assumed number of decay modes is bound to produce unreliable results.

Owing to the marked effect of modest molecular weight changes on the kinetic pathways, consensus about the equilibration mechanisms of copolymer micelles has been difficult to achieve on the grounds of results obtained from copolymers with different natures, compositions, architectures and molecular weights. This reflects the nature of a system that lacks a unique kinetic behaviour and that is the reason why the formulation of "one" *T*-jump protocol that will capture all the features (mechanisms) of the growth or decay of Pluronics or equivalent systems cannot be easily carried out.

Acknowledgements

We thank P. Mesini for clarifying discussion about the characterization of the samples by NMR, Y. Guilbert for running the NMR measurements, C. Foussat for performing the SEC characterization, and J.-P. Lamps for precious help in the chemistry lab. The research leading to these results has received funding from the People Programme (Marie Curie Actions) of the European Union's Seventh Framework Programme (FP7/2007–2013) under REA grant agreement no. PITN-GA-2012-317019 "TRACE and TREAT".

References

1 A. G. Denkova, E. Mendes and M.-O. Coppens, *Soft Matter*, 2010, **6**, 2351–2357.
2 T. Nicolai, O. Colombani and C. Chassenieux, *Soft Matter*, 2010, **6**, 3111–3118.
3 R. Lund, L. Willner and D. Richter, in *Controlled Polymerization and Polymeric Structures*, ed. A. Abe, K.-S. Lee, L. Leibler and S. Kobayashi, Springer International Publishing, 2013, vol. 259, pp. 51–158.
4 P. J. Flory, *Principles of Polymer Chemistry*, Cornell University Press, Ithaca, New York, 1953.
5 P. G. de Gennes, in *Solid State Physics*, ed. L. Liebert, Academic Press, New York, 1978, supp. 14, p. 1.
6 L. Zhang and A. Eisenberg, *Science*, 1995, **268**, 1728–1731.
7 E. A. G. Aniansson and S. N. Wall, *J. Phys. Chem.*, 1974, **78**, 1024–1030.
8 L. Willner, A. Poppe, J. Allgaier, M. Monkenbusch and D. Richter, *Europhys. Lett.*, 2001, **55**, 667.
9 Y.-Y. Won, H. T. Davis and F. S. Bates, *Macromolecules*, 2003, **36**, 953–955.
10 R. Lund, L. Willner, J. Stellbrink, P. Lindner and D. Richter, *Phys. Rev. Lett.*, 2006, **96**, 068302.
11 R. Lund, L. Willner, D. Richter and E. E. Dormidontova, *Macromolecules*, 2006, **39**, 4566–4575.
12 R. Lund, L. Willner, D. Richter, H. Iatrou, N. Hadjichristidis and P. Lindner, *J. Appl. Crystallogr.*, 2007, **40**, s327–s331.
13 S.-H. Choi, T. P. Lodge and F. S. Bates, *Phys. Rev. Lett.*, 2010, **104**, 047802.
14 R. Lund, L. Willner, J. Stellbrink, P. Lindner and D. Richter, *Phys. Rev. Lett.*, 2010, **104**, 049902.
15 R. Lund, L. Willner, V. Pipich, I. Grillo, P. Lindner, J. Colmenero and D. Richter, *Macromolecules*, 2011, **44**, 6145–6154.
16 T. Zinn, L. Willner, R. Lund, V. Pipich and D. Richter, *Soft Matter*, 2012, **8**, 623–626.
17 J. Lu, F. S. Bates and T. P. Lodge, *ACS Macro Lett.*, 2013, **2**, 451–455.
18 Y. Rharbi, *Macromolecules*, 2012, **45**, 9823–9826.
19 A. Halperin and S. Alexander, *Macromolecules*, 1989, **22**, 2403–2412.
20 E. Hecht and H. Hoffmann, *Colloids Surf., A*, 1995, **96**, 181–197.
21 B. Michels, G. Waton and R. Zana, *Langmuir*, 1997, **13**, 3111–3118.
22 I. Goldmints, J. F. Holzwarth, K. A. Smith and T. A. Hatton, *Langmuir*, 1997, **13**, 6130–6134.
23 G. Waton, *J. Phys. Chem. B*, 1997, **101**, 9727–9731.
24 G. Waton, B. Michels and R. Zana, *J. Colloid Interface Sci.*, 1999, **212**, 593–596.
25 M. J. Kositza, C. Bohne, P. Alexandridis, T. A. Hatton and J. F. Holzwarth, *Macromolecules*, 1999, **32**, 5539–5551.
26 M. J. Kositza, C. Bohne, P. Alexandridis, T. A. Hatton and J. F. Holzwarth, *Langmuir*, 1999, **15**, 322–325.
27 E. E. Dormidontova, *Macromolecules*, 1999, **32**, 7630–7644.
28 G. Waton, B. Michels and R. Zana, *Macromolecules*, 2001, **34**, 907–910.
29 T. Thurn, S. Couderc-Azouani, D. M. Bloor, J. F. Holzwarth and E. Wyn-Jones, *Langmuir*, 2003, **19**, 4363–4370.
30 R. Zana, C. Marques and A. Johner, *Adv. Colloid Interface Sci.*, 2006, **123–126**, 345–351.

31 K. Mortensen and W. Brown, *Macromolecules*, 1993, **26**, 4128–4135.
32 M. Duval, G. Waton and F. Schosseler, *Langmuir*, 2005, **21**, 4904–4911.
33 I. LaRue, M. Adam, M. Pitsikalis, N. Hadjichristidis, M. Rubinstein and S. S. Sheiko, *Macromolecules*, 2006, **39**, 309–314.
34 A. G. Denkova, E. Mendes and M.-O. Coppens, *J. Phys. Chem. B*, 2009, **113**, 989–996.
35 R. Ganguly, M. Kumbhakar and V. K. Aswal, *J. Phys. Chem. B*, 2009, **113**, 9441–9446.
36 Y. Kadam, R. Ganguly, M. Kumbhakar, V. K. Aswal, P. A. Hassan and P. Bahadur, *J. Phys. Chem. B*, 2009, **113**, 16296–16302.
37 G. Landazuri, V. V. A. Fernandez, J. F. A. Soltero and Y. Rharbi, *J. Phys. Chem. B*, 2012, **116**, 11720–11727.
38 R. Ganguly, K. Kuperkar, P. Parekh, V. Aswal and P. Bahadur, *J. Colloid Interface Sci.*, 2012, **378**, 118–124.
39 L. A. Fielding, J. A. Lane, M. J. Derry, O. O. Mykhaylyk and S. P. Armes, *J. Am. Chem. Soc.*, 2014, **136**, 5790–5798.
40 S. E. Burke and A. Eisenberg, *Langmuir*, 2001, **17**, 6705–6714.
41 R. Lund, L. Willner, D. Richter, P. Lindner and T. Narayanan, *ACS Macro Lett.*, 2013, **2**, 1082–1087.
42 I. Schmolka, *J. Am. Oil Chem. Soc.*, 1977, **54**, 110–116.
43 G. Wanka, H. Hoffmann and W. Ulbricht, *Colloid Polym. Sci.*, 1990, **268**, 101–117.
44 P. Alexandridis and T. A. Hatton, *Colloids Surf., A*, 1995, **96**, 1–46.
45 Z. Zhou and B. Chu, *Macromolecules*, 1987, **20**, 3089–3091.
46 V. V. A. Fernandez, J. F. A. Soltero, J. E. Puig and Y. Rharbi, *J. Phys. Chem. B*, 2009, **113**, 3015–3023.
47 S. Saeki, N. Kuwahara, M. Nakata and M. Kaneko, *Polymer*, 1977, **18**, 1027–1031.
48 Z. Zhou, B. Chu and D. G. Peiffer, *Macromolecules*, 1993, **26**, 1876–1883.
49 R. Klucker, J. P. Munch and F. Schosseler, *Macromolecules*, 1997, **30**, 3839–3848.
50 I. Echavarri Franco, P. Lorchat, J.-P. Lamps, M. Schmutz, A. Schröder, J.-M. Catala, J. Combet and F. Schosseler, *Langmuir*, 2012, **28**, 4815–4828.
51 M. Doi and S. F. Edwards, *The Theory of Polymer Dynamics*, Oxford University Press, 1986.
52 P. G. de Gennes, *Scaling Concepts in Polymer Physics*, Cornell University Press, Ithaca, New York, 1979.
53 B. J. Berne and R. Pecora, *Dynamic Light Scattering with Applications to Chemistry, Biology, and Physics*, Wiley Interscience, New York, 1976.
54 P. Alexandridis, J. F. Holzwarth and T. A. Hatton, *Macromolecules*, 1994, **27**, 2414–2425.

